AIP Applied Physics Letters

Position-controlled [100] InP nanowire arrays

Jia Wang, Sébastien Plissard, Moïra Hocevar, Thuy T. T. Vu, Tilman Zehender et al.

Citation: Appl. Phys. Lett. **100**, 053107 (2012); doi: 10.1063/1.3679136
View online: http://dx.doi.org/10.1063/1.3679136
View Table of Contents: http://apl.aip.org/resource/1/APPLAB/v100/i5
Published by the American Institute of Physics.

Related Articles

Electrical characteristics of cadmium doped InAs grown by metalorganic vapor phase epitaxy
J. Appl. Phys. 111, 023707 (2012)

Anisotropy of free-carrier absorption and diffusivity in m-plane GaN
Appl. Phys. Lett. 100, 022112 (2012)

Metalorganic chemical vapor deposition of N-polar GaN films on vicinal SiC substrates using indium surfactants
Appl. Phys. Lett. 100, 021913 (2012)

The influence of anisotropic gate potentials on the phonon induced spin-flip rate in GaAs quantum dots
Appl. Phys. Lett. 100, 023108 (2012)

The effect of InGaAs strain-reducing layer on the optical properties of InAs quantum dot chains grown on patterned GaAs(100)
J. Appl. Phys. 111, 014306 (2012)

Additional information on Appl. Phys. Lett.

Journal Homepage: http://apl.aip.org/
Journal Information: http://apl.aip.org/about/about_the_journal
Top downloads: http://apl.aip.org/features/most_downloaded
Information for Authors: http://apl.aip.org/authors

ADVERTISEMENT

Downloaded 30 Jan 2012 to 131.155.108.10. Redistribution subject to AIP license or copyright; see http://apl.aip.org/about/rights_and_permissions

APPLIED PHYSICS LETTERS **100**, 053107 (2012)

Position-controlled [100] InP nanowire arrays

Jia Wang,[1] Sébastien Plissard,[1] Moïra Hocevar,[2] Thuy T. T. Vu,[1] Tilman Zehender,[1] George G. W. Immink,[3] Marcel A. Verheijen,[1,3] Jos Haverkort,[1] and Erik P. A. M. Bakkers[1,2,a)]

[1]*Department of Applied Physics, Eindhoven University of Technology, P.O. Box 513, 5600 MB Eindhoven, The Netherlands*
[2]*Kavli Institute of Nanoscience, Delft University of Technology, 2628CJ Delft, The Netherlands*
[3]*Philips Innovation Services Eindhoven, High Tech Campus 11, 5656AE Eindhoven, The Netherlands*

(Received 25 November 2011; accepted 4 January 2012; published online 30 January 2012)

We investigate the growth of vertically standing [100] zincblende InP nanowire (NW) arrays on InP (100) substrates in the vapor-liquid-solid growth mode using low-pressure metal-organic vapor-phase epitaxy. Precise positioning of these NWs is demonstrated by electron beam lithography. The vertical NW yield can be controlled by different parameters. A maximum yield of 56% is obtained and the tapering caused by lateral growth can be prevented by *in situ* HCl etching. Scanning electron microscopy, high-resolution transmission electron microscopy, and micro-photoluminescence have been used to investigate the NW properties. © *2012 American Institute of Physics*. [doi:10.1063/1.3679136]

Indium phosphide (InP) nanowires (NWs) have attracted an increasing amount of attention because of their extensive use in electronics,[1] optoelectronics,[2,3] and photovoltaics,[4–6] and both axial[7,8] and core-shell[9] heterostructures have been developed for new advanced nanoscale devices. However, most NWs reported are grown in the direction perpendicular to that of the close-packed planes in the crystal structure, i.e., in the ⟨111⟩ direction for zincblende (ZB) or the ⟨0001⟩ direction for wurtzite (WZ), in which the NWs commonly have planar stacking faults (SFs), leading to a faulted crystal or even a mixture of ZB/WZ crystal structures.[10–15] Although SFs have been found to contribute to many phenomena,[12,15] they could significantly affect the electronic and optical properties[13,16–19] of nanowires. Zincblende nanowire growth in the ⟨100⟩ direction, which has seldom been reported for InP,[20] is of particular interest since such wires are inherently free from SFs and represents an ideal ZB single crystal. However, a systematic study of InP nanowires grown on InP (100) substrates with precise control of the position is still challenging and has not been reported yet.

In this work, we report on the growth of [100] ZB InP NWs by the vapor-liquid-solid (VLS) growth mechanism[21] catalyzed by Au and using low-pressure (50 mbar) metal-organic vapor phase epitaxy (MOVPE) on Sn-doped InP (100) substrates; this orientation has been mostly used in device applications. Electron beam lithography (EBL) is used to position the NWs since future device applications in optics as well as electronics require precise site control. Note that nano-imprint has been demonstrated to enable position control at the wafer level.[22] We demonstrate that the vertical NW growth direction on a (100) substrate depends strongly on parameters such as growth temperature, nanowire diameter, V/III ratio, and precursor molar fraction. *In situ* HCl etching is used to prevent lateral growth and to realize diameter uniformity along the NW axial direction.[23] Finally, we demonstrate control of position, diameter, length, yield, and tapering of defect-free pure zincblende [100] NW grown on InP (001) substrates.

The as-grown samples were studied using scanning electron microscopy (SEM) and transmission electron microscopy (TEM). For micro-photoluminescence (PL) measurements, the NWs were transferred to a thermally oxidized Si wafer. The micro-PL measurements were carried out at 4 K using a $100\times$ long distance objective. A diode laser (635 nm line) was used as excitation source, and the PL was detected by a cooled CCD detector.

In Figs. 1(a) and 1(b), SEM images of one NW field grown at 460 °C are shown. More than half of the e-beam defined Au particles grow into vertical [100] NWs (yield = 352/625 = 56.32%). As can be seen in close-up (Figs. 1(c) and 1(d)), all vertical NWs have a rectangular cross-sectional shape, similar to that in Ref. 20. The nature of the side facets was determined in two independent manners: (1) top-view SEM imaging, having the edges of the substrate for reference of the crystallographic orientation. (2) Using TEM, by a combination of electron diffraction and subsequent STEM/HAADF imaging to determine the brightness profile across the nanowire. Directly below the gold particle, an octagonal shape is present formed by four {110} and four {100} side facets. Further down the nanowire, lateral growth results in a morphology characterized by four {100} side facets instead of four {110} side facets as reported before.[20] These four {100} side facets are observed at most growth conditions. While at low V/III ratios (<160), four nonparallel (110) side facets are formed, and the nanowires maintain a quasi-octagonal cross-section. We argue that the P-terminated {100} facets are stabilized by the high V/III ratio. For the non-vertical wires, 3 different types of in-plane NW orientations can be found as shown by the marked wires in Fig. 1(b). The growth direction marked with 1 corresponds to growth in a ⟨111⟩B direction. The other two growth directions can be explained by a change in growth direction after a rotational twin boundary; NWs marked 2 and 3 grow in new ⟨100⟩ and ⟨111⟩ directions after this twin,

a)Electronic mail: e.p.a.m.bakkers@tue.nl.

 © 2012 American Institute of Physics

Downloaded 30 Jan 2012 to 131.155.108.10. Redistribution subject to AIP license or copyright; see http://apl.aip.org/about/rights_and_permissions

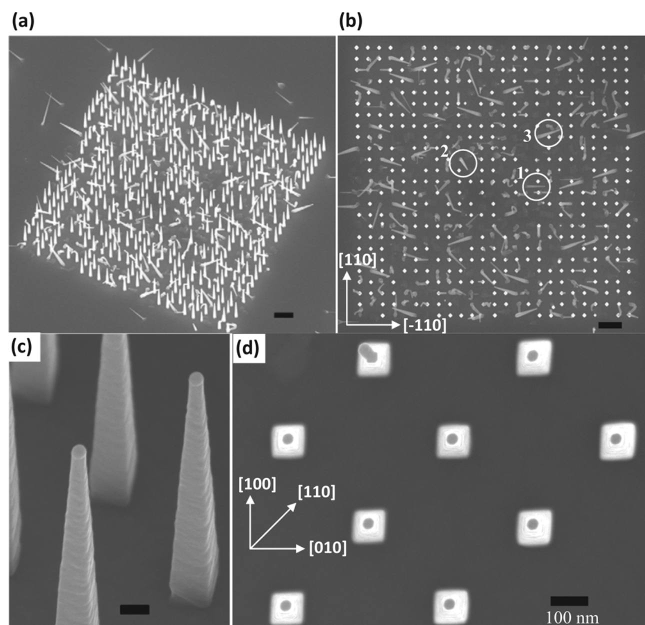

FIG. 1. SEM images of as-grown InP NW arrays on a InP (100) substrate with Au diameters (D_{Au}) = 50 nm, pitch = 500 nm, growth temperatures (T) = 460 °C, V/III ratio = 229, and standard total molar fraction (F_{total}). (a), (c) View on a substrate tilted by 40°. (b), (d) Top-view images showing the square shape of vertical NWs with {100} side facets. Circular marks in (b) show three different tilted growth directions. The scale bar is 1 μm for (a), (b) and 100 nm for (c), (d).

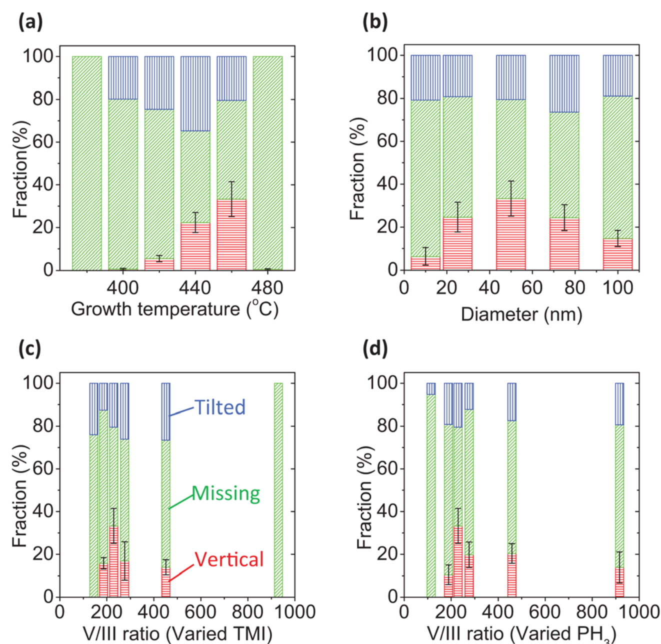

FIG. 2. (Color online) Histograms of vertical, tilted, and missing NW fractions varying with different parameters: (a) with D_{Au} = 50 nm, V/III ratio = 229, varying T. (b) With V/III ratio = 229, T = 460 °C, varying D_{Au}. (c) D_{Au} = 50 nm, T = 460 °C, molar fraction of PH_3 (F_{PH3}) = 5.5×10^{-3}, with varying V/III ratio by changing TMI molar fraction (F_{TMI}). (d) D_{Au} = 50 nm, T = 460 °C, $F_{TMI} = 3.8 \times 10^{-5}$, with varying V/III ratio by changing F_{PH3}. The error bars indicate the standard deviation of our measurements.

respectively. For type 2 and 3, the four in-plane directions are 45° and 70° off [110], respectively, and the angles with the surface normal are 20° and 72°, respectively. The further details of the different growth directions are out of the scope of this paper.

For each sample, the yield of more than 3 NW fields (each containing 625 NWs) from different areas over the wafer was measured by using SEM. The yield is strongly affected by the growth temperature as can be seen in Fig. 2(a). Here, patterned Au island diameters (D_{Au}) = 50 nm, V/III ratio = 229, and standard precursor molar fractions ($F_{TMI} = 3.8 \times 10^{-5}$ and $F_{PH3} = 5.5 \times 10^{-3}$) are used. At too low (380 °C) or too high (480 °C) temperatures NWs do not grow at all. At 400 °C almost all wires are grown in tilted directions. Vertically [100]-oriented wires were found in the range 420–460 °C with a maximum at 460 °C. We find an optimum temperature for vertical growth above the Au-In eutectic temperature (T = 454 °C). Though the sample temperature is higher than 454 °C, vertical NW growth was still found. This indicates that the proposed mechanism for vertical wire growth on [100] substrates,[20] which is based on preventing the formation of an alloy between the Au particle and the substrate, is not valid under our growth conditions. In an additional experiment the sample was pre-annealed at 550 °C for 10 min before growth. This did not significantly affect the yield of vertical wires, supporting our conclusion. In Fig. 2(b) the yield of vertical wires is plotted as a function of the diameter. The highest fraction is obtained for D_{Au} = 50 nm, while the fraction of tilted NWs is not affected by the diameter. The fraction of vertical NWs is also affected by the V/III ratio as shown in Figs. 2(c) and 2(d). In these graphs the yield is given for a varied F_{TMI} (or F_{PH3}) but a fixed F_{PH3} (or F_{TMI}). Below a critical total molar fraction ($F_{TMI} = 3.9 \times 10^{-5}$ and $F_{PH3} = 5.5 \times 10^{-3}$), there are no vertical NWs grown. If it is decreased further, keeping the same V/III ratio, no NW growth is observed. Finally, it was found that the yield is independent of the wire-to-wire distance, indicating that the V/III ratio does not change with the wire-to-wire distance under these growth conditions. In other words, the diffusion length of the precursors on the InP (100) is either much longer or shorter than the wire-to-wire distance used in this work. We note that all the samples were coated with a thin film of poly-L-lysine (PLL), which could change surface energies, and with that the shape of the droplet shape;[24] without PLL coating, the vertical NW yield is reduced by 10%.

In order to verify the NW crystalline structure, TEM studies were performed for ten NWs. Fig. 3(a) shows a bright field TEM image of a typical [100] InP NW deposited on a holey carbon film. The defect-free pure ZB crystal structure of the wire is clear from the high resolution TEM image in Fig. 3(b). Note that twin boundaries (parallel to {111} lattice planes) are well recognizable both in [011] as well as in [001] zone-axis imaging and have not been observed here. The optical properties of single [100] wires are investigated by low-temperature micro-PL (Fig. 3(c)). At the lowest excitation power used here (2.4 W/cm^{-2}) a peak (II) at 1.415 eV was observed, with a full width at half maximum (FWHM) of 2.3 meV. This peak is 5 meV below the band-gap energy of zincblende InP (1.42 eV) and assigned to a donor-to-valence band transition. The peaks from 1.36–1.40 eV are assigned to impurity-related emission. Note that no strong emission around 1.38 eV is observed, typical for a conduction band-to-acceptor transition due to carbon impurity, even

Downloaded 30 Jan 2012 to 131.155.108.10. Redistribution subject to AIP license or copyright; see http://apl.aip.org/about/rights_and_permissions

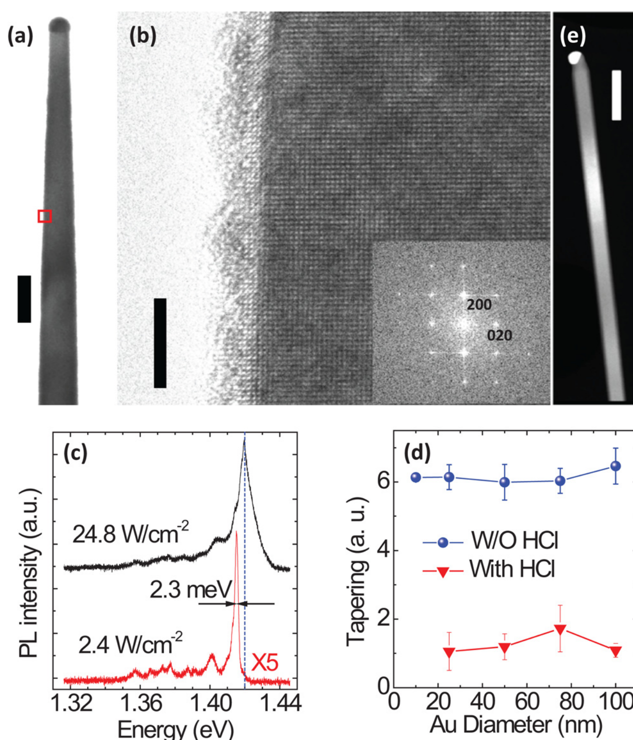

FIG. 3. (Color online) (a) Bright-field TEM image of a [100] InP NWs. (b) HRTEM image of the boxed area. The inset shows the Fourier transform of the HRTEM image, displaying a [001] zone axis pattern. (c) PL at 4 K from a single [100] InP NW transferred to an oxidized Si wafer. (d) Effect of HCl on InP NW tapering. (e) High angle annular dark field STEM image of a [100] InP NW grown with HCl at partial pressure 8.33×10^{-4} mbar. The scale bar is 100 nm for (a),(e) and 5 nm for (b).

though the NWs are grown at a relatively low growth temperature (460 °C). With 24.8 W/cm^{-2} excitation power, the band-gap related PL of the same NW is at 1.42 eV.

Finally, in order to reduce undesired lateral growth and realize uniformity along the [111] direction, *in situ* HCl etching is used as shown for [111] NW.[23] HCl is simultaneously switched on and off with TMI. Fig. 3(d) shows that all NWs grown without HCl are tapered, independently of the diameter (tapering is defined as the difference between the bottom and top NW diameter divided by its length: $(D_b\text{-}D_t)/L$). Nearly untapered wires are obtained by using an HCl partial pressure of 8.33×10^{-4} mbar, as can be seen in Fig. 3(e).

As already visible from SEM studies, NW growth without HCl yields {100} facets upon lateral growth. On the contrary, NW growth with HCl yields an octagonal shape formed by four {110} and four {100} side facets, as confirmed by a more detailed TEM study. A detailed analysis of the effect of HCl will be presented elsewhere.

In conclusion, [100] InP NWs with more than 50% yield have been fabricated with optimized growth parameters on (100) InP substrates grown by MOVPE. The NW's cross-sectional shape can be tuned by using HCl. These defect-free pure ZB wires have high optical quality as concluded from the sharp emission peak (FWHM = 2.3 meV) and are a promising platform for the integration of InAsP quantum dots.[25] It allows to precisely tuning the cross-sectional shape and length to tailor and minimize the fine structure splitting.[26]

[1] X. F. Duan, Y. Huang, Y. Cui, J. F. Wang, and C. M. Lieber, Nature **409**, 66 (2001).
[2] J. Wang, M. S. Gudiksen, X. Duan, Y. Cui, and C. M. Lieber, Science **24**, 1455 (2001).
[3] Y. Ding, J. Motohisa, B. Hua, S. Hara, and T. Fukui, Nano Lett. **7**, 3598 (2007).
[4] R. Yan, D. Gargas, and P. Yang, Nat. Photon. **3**, 569 (2009).
[5] H. Goto, K. Nosaki, K. Tomioka, S. Hara, K. Hiruma, J. Motohisa, and T. Fukui, Appl. Phys. Express **2**, 035004 (2009).
[6] M. T. Borgström, J. Wallentin, M. Heurlin, S. Fält, P. Wickert, J. Leene, M. H. Magnusson, K. Deppert, and L. Samuelson, IEEE J. Sel. Top. Quantum Electron. **17**, 1050 (2010).
[7] M. T. Björk, B. J. Ohlsson, C. Thelander, A. I. Persson, K. Deppert, L. R. Wallenberg, and L. Samuelson, Appl. Phys. Lett. **81**, 4458 (2002).
[8] E. D. Minot, F. Kelkensberg, M. van Kouwen, J. A. van Dam, L. P. Kouwenhoven, V. Zwiller, M. T. Borgström, O. Wunnicke, M. A. Verheijen, and E. P. A. M. Bakkers, Nano Lett. **7**, 367 (2007).
[9] P. Mohan, J. Motohisa, and T. Fukui, Appl. Phys. Lett. **88**, 133105 (2006).
[10] S. Bhunia, T. Kawamura, S. Fujikawa, H. Nakashima, K. Furukawa, K. Torimitsu, and Y. Watanabe, Thin Solid Films **464**, 244 (2004).
[11] Q. Xiong, J. Wang, and P. C. Eklund, Nano Lett. **6**(12), 2736 (2006).
[12] R. E. Algra, M. A. Verheijen, M. T. Borgström, L. Feiner, G. Immink, W. J. P. van Enckevort, E. Vlieg, and E. P. A. M. Bakkers, Nature **456**, 369 (2008).
[13] J. Bao, D. C. Bell, F. Capasso, J. B. Wagner, T. Mårtensson, J. Trägårdh, and L. Samuelson, Nano Lett. **8**, 836 (2008).
[14] K. Ikejiri, Y. Kitauchi, K. Tomioka, J. Motohisa, and T. Fukui, Nano Lett. **11**(10), 4314 (2011).
[15] N. Akopian, G. Patriarche, L. Liu, J. C. Harmand, and V. Zwiller, Nano Lett. **10**, 1198 (2010).
[16] Z. Ikonic, G. P. Srivastava, and J. C. Inkson, Phys. Rev. B **52**, 14078 (1995).
[17] M. D. Schroer and J. R. Petta, Nano Lett. **10**, 1618 (2010).
[18] S. A. Dayeh, D. Susac, K. L. Kavanagh, E. T. Yu, and D. Wang, Adv. Funct. Mater. **19**, 2102 (2009).
[19] C. Thelander, P. Caroff, S. Plissard, A. W. Dey, and K. A. Dick, Nano Lett. **11**, 2424 (2011).
[20] U. Krishnamachari, M. Borgstrom, B. J. Ohlsson, N. Panev, L. Samuelson, W. Seifert, M. W. Larsson, and L. R. Wallenberg, Appl. Phys. Lett. **85**, 2077 (2004).
[21] R. S. Wagner and W. C. Ellis, Appl. Phys. Lett. **4**, 89 (1964).
[22] A. Pierret, M. Hocevar, S. L Diedenhofen, R. E Algra, E. Vlieg, E. C. Timmering, M. A. Verschuuren, G. W. G. Immink, M. A Verheijen, and E. P. A. M. Bakkers, Nanotechnology **21**, 065305 (2010).
[23] M. T. Borgström, J. Wallentin, J. Trägårdh, P. Ramvall, M. Ek, L. R. Wallenberg, L. Samuelson, and K. Deppert, Nano Res. **3**, 264 (2010).
[24] A. Mikkelsen, J. Eriksson, E. Lundgren, J. N. Andersen, J. Weissenrieder, and W. Seifert, Nanotechnology **16**, 2354 (2005).
[25] M. H. M. van Weert, N. Akopian, U. Perinetti, M. P. van Kouwen, R. E. Algra, M. A. Verheijen, E. P. A. M. Bakkers, L. P. Kouwenhoven, and V. Zwiller, Nano Lett. **9**, 1989 (2009).
[26] R. Singh and G. Bester, Phys. Rev. Lett. **103**, 063601 (2009).

Downloaded 30 Jan 2012 to 131.155.108.10. Redistribution subject to AIP license or copyright; see http://apl.aip.org/about/rights_and_permissions